ACS APPLIED MATERIALS & INTERFACES

Research Article

www.acsami.org

Ultrathin β-Ni(OH)$_2$ Nanoplates Vertically Grown on Nickel-Coated Carbon Nanotubes as High-Performance Pseudocapacitor Electrode Materials

Xiaowei Ma,[†] Ying Li,[†] Zhiwei Wen,[‡] Fengxia Gao,[†] Chongyun Liang,[‡] and Renchao Che*[,†,‡]

[†]Laboratory of Advanced Materials and [‡]Department of Materials Science, Fudan University, Shanghai, 200433, People's Republic of China

Supporting Information

ABSTRACT: Various metal hydroxides/oxides grown on conductive substrates such as nickel foam have been reported and studied as supercapacitor electrode materials. However, the capacitances of these electrodes are extremely limited because of the low content of active materials grown on the limited surface of nickel foam. To achieve high capacitance, we use nickel-coated carbon nanotubes (Ni-CNTs) as the conductive substrate for the growth of β-Ni(OH)$_2$. By a facile chemical method, ultrathin β-Ni(OH)$_2$ nanoplates are vertically grown on the surface of Ni-CNTs. The density, thickness, and content of β-Ni(OH)$_2$ can be easily controlled by modulating the ratio of NiCl$_2$·6H$_2$O to Ni-CNTs. This hierarchical nanostructure can provide remarkable synergistic effects: facilitate electron and ion transport and accelerate the reversible redox reactions. As-prepared Ni-CNTs@β-Ni(OH)$_2$ composites exhibit high specific capacitances (~1807 F g^{-1} at 2 A g^{-1}, based on the mass of β-Ni(OH)$_2$; ~1283 F g^{-1} at 2 A g^{-1}, based on the mass of composite), good rate capabilities, and excellent cycling stabilities. This strategy has potential for large-scale production and can be applied to the preparation of other hierarchical nanostructured metal hydroxide/oxide composites.

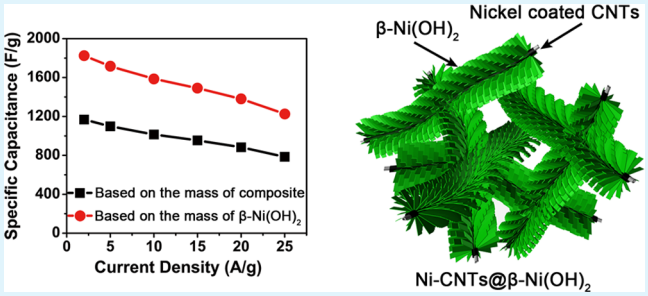

KEYWORDS: *β-nickel hydroxide, nickel-coated carbon nanotubes, three-dimensional conductive substrate, supercapacitor, hierarchical nanostructure*

1. INTRODUCTION

Metal hydroxides and oxides are considered the most promising electrode materials for pseudocapacitors.[1] Various metal hydroxides/oxides have been reported and studied as pseudocapacitor electrode materials, such as Co(OH)$_2$,[2−4] Ni(OH)$_2$,[5−7] Co$_3$O$_4$,[8−10] NiO,[11−15] and RuO$_2$.[16,17] Compared with electrochemical double-layer capacitors, pseudocapacitors possess higher energy densities because pseudocapacitances based on the fast and reversible redox reactions of active materials are much higher than double-layer capacitances mainly based on ion absorption. The fast and reversible redox reactions mainly take place at the surfaces or near-surface regions of active materials especially under fast charge/discharge conditions. To make full use of active materials and achieve high performance, their morphologies are always designed to shorten or provide sufficient ion-transport pathways, such as nanosized or porous structures. For example, various nanostructured Ni(OH)$_2$ including nanoplates,[5,18] nanoflowers,[19,20] and hierarchical nanostructures[21,22] have been reported as high-performance supercapacitor electrode materials.

Although these special designed nanostructures can efficiently shorten ion-transport pathways, the poor electronic conductivities of metal hydroxides/oxides significantly hinder electron transport and decelerate redox reactions, always resulting in low capacitances and bad rate capabilities. The most commonly used strategy for improving their electronic conductivities is to combine them with conductive substrates, such as carbon materials,[23,24] conducting polymers,[25,26] and even current collectors.[12,18] Carbon materials, mainly including activated carbon, carbon nanotubes, and graphene, are the most frequently used conductive substrates because of their high specific surface areas, good electronic conductivities, and great chemical stabilities. However, the direct growth of metal hydroxides/oxides on carbon materials is difficult because their surfaces are not compatible. To improve their surface compatibility, oxidative treatments of carbon materials are always necessary, which could introduce numerous structural defects and oxygen-containing groups facilitating the growth of metal hydroxides/oxides on the surfaces of carbon materials.[27] In the case of current collectors such as nickel foam or fluorine-doped tin oxide glass (FTO), the direct growth of metal hydroxides/oxides can be easily achieved because the metal atoms or oxide atoms can provide remarkable compatibility

Received: November 5, 2014
Accepted: December 16, 2014
Published: December 16, 2014

DOI: 10.1021/am5077183
ACS Appl. Mater. Interfaces 2015, 7, 974−979

between their surface.[12] However, the content of active material is always extremely limited due to the limited specific surface area of nickel foam (or FTO) and the limited coating thickness of active material. As a result, the capacitance of electrode is unsatisfactory.

In this work, we used nickel-coated carbon nanotubes (Ni-CNTs) as the conductive substrate for the growth of β-$Ni(OH)_2$. By a facile chemical method, ultrathin β-$Ni(OH)_2$ nanoplates were vertically grown on the surface of Ni-CNTs. The morphology and content of β-$Ni(OH)_2$ could be controlled by modulating the ratio of $NiCl_2{\cdot}6H_2O$ to Ni-CNTs. Benefiting from the remarkable synergistic effects provided by the hierarchical nanostructure, as-prepared Ni-CNTs@β-$Ni(OH)_2$ composites exhibited high specific capacitances (~1807 F g^{-1} at 2 A g^{-1}, based on the mass of β-$Ni(OH)_2$; ~1283 F g^{-1} at 2 A g^{-1}, based on the total mass of composite), good rate capabilities, and excellent cycling stabilities.

2. EXPERIMENTAL SECTION

2.1. Preparation of Ni-CNTs@α-$Ni(OH)_2$ Composites. Ni-CNTs were purchased from Chengdu Organic Chemicals Co. Ltd., Chinese Academy of Sciences. $NiCl_2{\cdot}6H_2O$ (1.0, 1.25, and 1.5 mmol for three samples with different diameter) was dissolved in 30 mL of diethylene glycol (DEG). Then 80 mg of Ni-CNTs was dispersed into the solution by 30 min of ultrasonication. NaAc/DEG solution (10 mL, 0.2 g mL^{-1}) was added into the dispersion. Finally, the mixture was sealed into a 50 mL Teflon-lined stainless-steel autoclave for solvothermal reaction at 180 °C for 10 h. The final product was collected by centrifuge and rinsed with water and ethanol.

2.2. Preparation of Ni-CNTs@β-$Ni(OH)_2$ Composites. 40 mg of Ni-CNTs@α-$Ni(OH)_2$ was dispersed into 40 mL of NaOH aqueous solution (100 mmol L^{-1}). Then the dispersion was sealed into a 50 mL Teflon-lined stainless-steel autoclave for hydrothermal reaction at 180 °C for 1 h. The final product was collected by centrifuge and washed with ethanol. All the products were dried at 80 °C overnight.

2.3. Characterization. Powder X-ray diffraction (XRD) measurements were carried out using a Bruker D8 X-ray diffractometer with Ni-filtered Cu Kα radiation (40 kV, 40 mA). Transmission electron microscopy (TEM) was performed on a JEOL JEM-2100F transmission electron microscope. Field-emission scanning electron microscopy (SEM) images were acquired on a S-4800 field-emission scanning electron microscope operated at 1.0 kV. Thermal gravimetric analysis (TGA) data were recorded at a heating rate of 10 °C min^{-1} in air by a simultaneous thermogravimetry/differential thermal analyzers (DTG-60H).

2.4. Electrochemical Measurements. The working electrode was prepared as follows. First, active material powder, acetylene black, and poly(tetrafluoroethylene), with a weight ratio of 80:10:10, were mixed; then the mixture was pressed into a film and dried in oven at 80 °C overnight. Then the film was cut into small pieces. Finally, the working electrode was prepared by pressing one small piece (1–2 mg) onto nickel foam at a pressure of 10 MPa. The electrochemical tests were conducted on a CHI 660D electrochemical workstation. The electrochemical studies of the individual electrode were performed in a three-electrode cell, where Pt foil serves as the counter electrode and a Hg/HgO electrode serves as the reference electrode. KOH aqueous solution (1 M) was used as the electrolyte. Nyquist plots were taken from 0.1 Hz to 100 kHz and analyzed by software ZsimpWin.

3. RESULTS AND DISCUSSION

Ni-CNTs@β-$Ni(OH)_2$ composite was prepared via a facile chemical method as previously reported.[20] First, Ni-CNTs@α-$Ni(OH)_2$ composite was prepared by a solvothermal reaction at 180 °C; then it was transformed into Ni-CNTs@β-$Ni(OH)_2$ after a hydrothermal reaction in alkaline solution. The two-step synthesis method was chosen for two main reasons: (1) β-$Ni(OH)_2$ shows better stability and higher discharge voltage, while α-$Ni(OH)_2$ is not stable in alkaline solution resulting in serious capacitance decay during electrochemical cycling;[28] (2) this method can ensure uniform β-$Ni(OH)_2$ coating grown on Ni-CNTs. β-$Ni(OH)_2$ could be easily synthesized via one-step hydrothermal reaction; however, the too-high reaction rate would result in nonuniform growth of β-$Ni(OH)_2$ on Ni-CNTs and isolated β-$Ni(OH)_2$ nanoparticles, which could be difficult to eliminate from this system. And this would lead to high electronic resistance of composite, which is adverse to its electrochemical performance.

After a solvothermal reaction at 180 °C for 10 h, Ni-CNTs@α-$Ni(OH)_2$ composite was obtained. Its XRD spectrum is shown in Figure 1 (black line). All the diffraction peaks can be

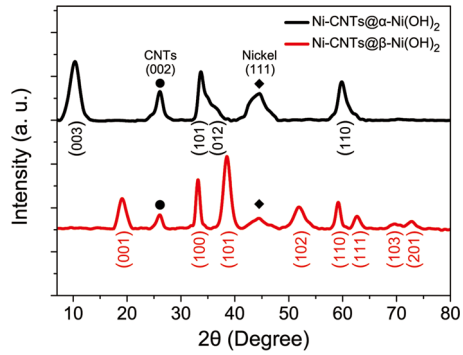

Figure 1. XRD spectra of Ni-CNTs@α-$Ni(OH)_2$ (black line) and Ni-CNTs@β-$Ni(OH)_2$ (red line).

well-indexed to the CNTs-(002) peak, the Ni-(111) peak, and α-$Ni(OH)_2$ (JCPDS No. 38–0715). The transformation from Ni-CNTs@α-$Ni(OH)_2$ to Ni-CNTs@β-$Ni(OH)_2$ could be completed within 1 h confirmed by the XRD spectrum of Ni-CNTs@β-$Ni(OH)_2$ (Figure 1, red line). After a hydrothermal reaction in alkaline solution for 1 h, all the diffraction peaks belonging to α-$Ni(OH)_2$ disappeared. Except for the CNTs-(002) peak and the Ni-(111) peak, all the diffraction peaks can be ascribed to β-$Ni(OH)_2$ (JCPDS No. 14–0117) indicating the complete transformation. The XRD spectra of Ni-CNTs@β-$Ni(OH)_2$ composites with different β-$Ni(OH)_2$ content were shown in Supporting Information, Figure S1. Their diffraction peaks were similar except that the relative intensities of the CNTs-(002) peak were different implying their different content of β-$Ni(OH)_2$.

The morphologies of as-prepared composites were characterized by field-emission scanning electron microscopy (SEM). After Ni-CNTs@α-$Ni(OH)_2$ transformed into Ni-CNTs@β-$Ni(OH)_2$, there was no significant morphological change (Figure 2). One possible reason was that the hydrothermal reaction time was too short (only 1 h) for significant morphological changes. Another possible reason was that the platelike morphology of α-$Ni(OH)_2$ was similar to the morphology of single-crystalline β-$Ni(OH)_2$.[5] As previously reported,[20] the strain introduced by distorted morphology was the main cause for morphological changes after α-$Ni(OH)_2$ transformed into β-$Ni(OH)_2$. However, there was little strain in the α-$Ni(OH)_2$ nanoplates. Consequently, no significant morphological change was observed.

The β-$Ni(OH)_2$ coating consisted of numerous β-$Ni(OH)_2$ nanoplates, which were almost vertically grown on the surface

DOI: 10.1021/am5077183
ACS Appl. Mater. Interfaces 2015, 7, 974–979

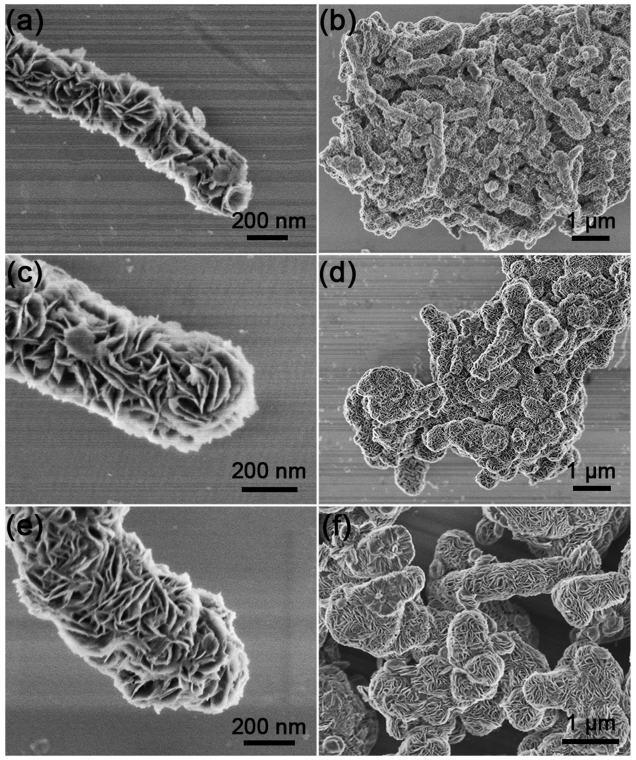

Figure 2. (a, b) SEM images of sample **a** with an average diameter of ~300 nm; (c, d) SEM images of sample **b** with an average diameter of ~400 nm; (e, f) SEM images of sample **c** with an average diameter of ~500 nm.

of Ni-CNTs (Figure 2). As shown in Supporting Information, Figure S2, the thickness of β-$Ni(OH)_2$ nanoplates was only few nanometers (~5−10) greatly shortening ion-transport pathways. The diameter of Ni-CNTs@β-$Ni(OH)_2$ rods could be controlled from ~300 to ~500 nm by modulating the ratio of $NiCl_2{\cdot}6H_2O$ to Ni-CNTs, while the content of β-$Ni(OH)_2$ could be increased from 49 wt % to 71 wt %. When the diameter was ~300 nm, the β-$Ni(OH)_2$ coating was thin and loose (Figure 2a). This morphology could not make full use of the conductive substrate and resulted in lower specific capacitances. As the diameter increased, the β-$Ni(OH)_2$ coating became denser and thicker (Figure 2c,e). Both the morphology and content of β-$Ni(OH)_2$ showed important influence on the electrochemical performance of as-prepared composite. This hierarchical nanostructure could provide remarkable synergistic effects: facilitate electron and ion transport, and accelerate the reversible redox reactions (Scheme 1).

Interestingly, single Ni-CNTs@β-$Ni(OH)_2$ rods were not common in as-prepared composites characterized by SEM and transmission electron microscopy (TEM, Supporting Information, Figure S3). In contrast, there were many large blocks constructed of considerable Ni-CNTs@β-$Ni(OH)_2$ rods. Actually, these large blocks were not simply stacked or assembled from single Ni-CNTs@β-$Ni(OH)_2$ rods but from cohesive wholes. The root cause was that considerable Ni-CNTs were connected by the nickel coating and formed three-dimensional connected substrates for the growth of β-$Ni(OH)_2$ (Supporting Information, Figure S4). The nickel coating of Ni-CNTs was continuous on the surface of CNTs even at the intersections of CNTs and connected CNTs up through these intersections (Scheme 1). This three-dimensional (3D) connected Ni-CNTs served as 3D conductive network in

Scheme 1. Schematic Illustration for the Structures of Ni-CNTs@β-$Ni(OH)_2$ Composites and the Mechanism of Their Synergistic Effect

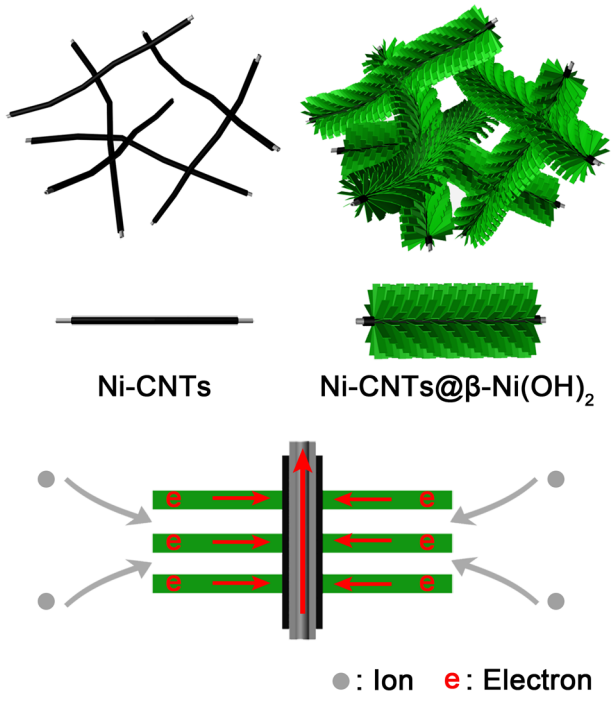

composites and efficiently enhanced their electronic conductivities.

Because of the different contents of β-$Ni(OH)_2$, three Ni-CNTs@β-$Ni(OH)_2$ samples showed quite different specific capacitances based on the mass of composites (Figure 3a). Sample **c** (~500 nm) exhibited the highest specific capacitance ~1283 F g^{-1} at 2 A g^{-1}, while the specific capacitances of the other two samples were 1168 and 887 F g^{-1} at 2 A g^{-1}, respectively. Sample with higher β-$Ni(OH)_2$ content would show higher specific capacitance, because the pseudocapacitance contributed by the redox reactions was far higher than the double-layer capacitance.[1] However, the specific capacitance of sample **c** (~500 nm) dropped much faster as current density increased and was much lower than that of sample **b** (~400 nm) at 25 A g^{-1}. This was perhaps because the electron-transport pathway was lengthened and ion-diffusion processes in electrolyte were hindered as the β-$Ni(OH)_2$ coating became much denser and thicker. The electron-transport process was limited by the thickness of β-$Ni(OH)_2$ coating (i.e., the size of β-$Ni(OH)_2$ nanoplates vertically grown on Ni-CNTs) because the electron-transport pathways were along the β-$Ni(OH)_2$ nanoplates (Scheme 1). The denser β-$Ni(OH)_2$ coating would provide less space for electrolyte storage and decrease ion-diffusion pathways, even block some of them.[33] Therefore, it can be concluded that the increase of β-$Ni(OH)_2$ content could indeed lead to high specific capacitance at low current density, but it would reduce the synergistic effect and hinder electron-transport and ion-diffusion processes, resulting in serious capacitance drop as current density increased.

Compared with sample **c** (~500 nm), sample **b** (~400 nm) showed slightly lower specific capacitances at low current densities but higher specific capacitances at high current densities revealing its better rate capability (Figure 3a). It was indicated that both the morphology and content of β-$Ni(OH)_2$ had important influence on the electrochemical performance of

DOI: 10.1021/am5077183
ACS Appl. Mater. Interfaces 2015, 7, 974−979

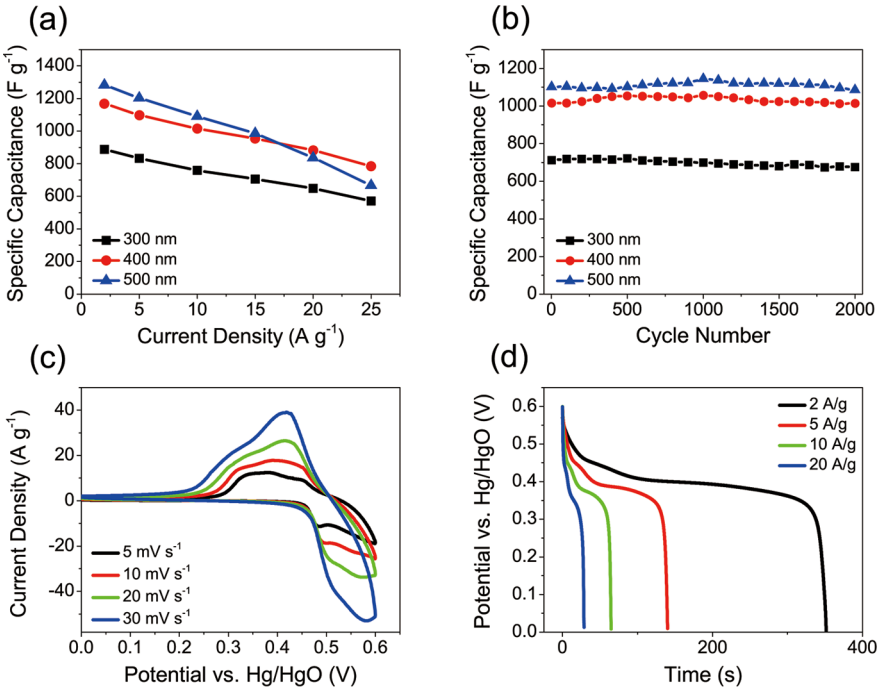

Figure 3. (a) Specific capacitances of three Ni-CNTs@β-Ni(OH)$_2$ samples at different current densities. (b) Cycling performances of three Ni-CNTs@β-Ni(OH)$_2$ at 10 A g^{-1}. (c) CV curves of sample **b** (400 nm) at different scan rates. (d) Galvanostatic charge/discharge curves of sample **b** (400 nm) at different current densities.

Ni-CNTs@β-Ni(OH)$_2$ composite. In spite of the significant differences in their specific capacitances, three Ni-CNTs@β-Ni(OH)$_2$ samples all exhibited good cycling stabilities (Figure 3b). After 2000 cycles at 10 A g^{-1}, their capacitance retentions were ~95, ~100, and ~98%, respectively. The performances of Ni-CNTs and β-Ni(OH)$_2$ were shown in Supporting Information, Figures S6 and S7, indicating that our strategy was successful and could efficiently enhance the performance of Ni-CNTs@β-Ni(OH)$_2$ composites.

β-Ni(OH)$_2$ is a typical pseudocapacitive material with definite oxidation and reduction potentials. Figure 3c shows the CV curves of sample **b** (400 nm) at different scan rates. A couple of well-defined redox current peaks could be observed, corresponding to the reversible redox reaction of β-Ni(OH)$_2$ ↔ β-NiOOH.[29,30] Its charge/discharge curves at different current densities are shown in Figure 3d. The charge and discharge voltage plateaus were ~0.52 and 0.41 V (vs Hg/HgO) at 2 A g^{-1}. As the current density increased from 2 to 20 A g^{-1}, the positions of its charge and discharge voltage plateaus showed slight changes implying sample **b** (400 nm) possessed good electronic conductivity, fast ion diffusion, and low equivalent series resistance.[31]

Although three Ni-CNTs@β-Ni(OH)$_2$ samples showed quite different specific capacitances based on the mass of composites, they showed some similarities in their specific capacitances based on the mass of β-Ni(OH)$_2$. As shown in Figure 4, the specific capacitances based on the mass of β-Ni(OH)$_2$ were similar when the current density was low (~1734, ~1716, and ~1694 F g^{-1} at 5 A g^{-1}, respectively). However, as the current density increased, sample **c** (500 nm) showed more serious capacitance drop. At a current density of 25 A g^{-1}, the specific capacitance of sample **c** (500 nm) was only ~938 F g^{-1}, much lower than those of the other two samples (~1190 and ~1226 F g^{-1}, respectively). Compared with sample **b** (400 nm), sample **a** (300 nm) showed slightly

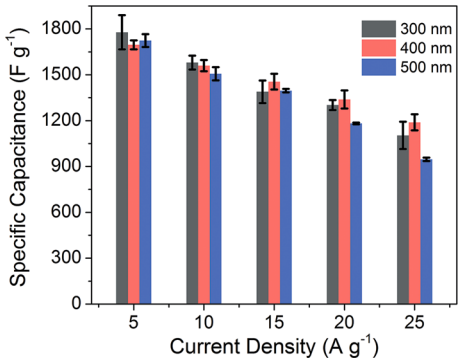

Figure 4. Specific capacitances (based on the mass of β-Ni(OH)$_2$) of three Ni-CNTs@β-Ni(OH)$_2$ samples at different current densities. Their weight contents of β-Ni(OH)$_2$ were ~49%, 64%, and 71%.

lower specific capacitance. This was probably caused by the imperfect coating of β-Ni(OH)$_2$ on Ni-CNTs, which could reduce the synergistic effect resulting lower electronic conductivity.

To further study the electrochemical properties of these Ni-CNTs@β-Ni(OH)$_2$ samples, electrochemical impedance spectroscopy (EIS) was conducted in the frequency range from 0.1 Hz to 100 kHz. Figure 5 shows the Nyquist plots of three Ni-CNTs@β-Ni(OH)$_2$ samples. Each plot is a plot of the imaginary part (Z″) of the impedance against the real part (Z′) and can be characterized by two distinct parts: a semicircle at high frequency and a straight line at low frequency.[34] The diameter of the semicircle corresponds to the charge-transfer resistance for the redox reactions at the electrode/electrolyte interface.[1] The straight line is associated with the ion-diffusion process between Warburg diffusion and ideal capacitive ion diffusion (pseudocapacitance).[32−34]

DOI: 10.1021/am5077183
ACS Appl. Mater. Interfaces 2015, 7, 974−979

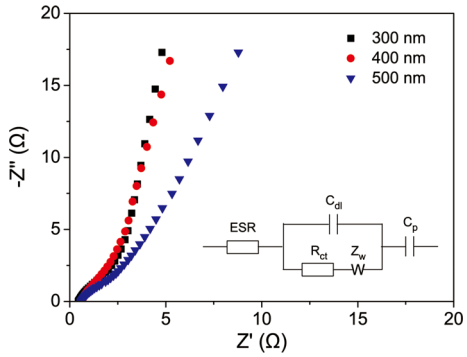

Figure 5. Nyquist plots of three Ni-CNTs@β-Ni(OH)$_2$ samples. (inset) The equivalent circuit (modified Randles equivalent circuit).

All these EIS data can be well-fitted to modified Randles equivalent circuit, where ESR is the equivalent series resistance, R_{ct} is the charge-transfer resistance, Z_w is the Warburg impedance, C_{dl} is the double-layer capacitance, and C_p is the pseudocapacitance. Calculated from the EIS data, the charge-transfer resistances of three samples are 0.61, 0.59, and 0.93 Ω, respectively. The low transfer resistances indicated that our strategy could effectively enhance the conductivity and facilitate the redox reactions at the electrode/electrolyte interface. The relatively higher charge-transfer resistance of sample **c** (500 nm) was caused by its thicker β-Ni(OH)$_2$ coating.

In general, the larger slope of the straight line corresponds to lower Warburg impedance and better ion diffusion. Both sample **a** (300 nm) and sample **b** (400 nm) showed low Warburg impedances implying their fast ion-diffusion processes. As the β-Ni(OH)$_2$ coating of sample **c** (500 nm) became much denser and thicker, the ion-diffusion process was hindered, and its plot exhibited a smaller slope. Slow ion-diffusion process and higher charge-transfer resistance were probably two main reasons for its serious capacitance drop as current density increased.

Detailed information about impedances of three Ni-CNTs@β-Ni(OH)$_2$ samples obtained from EIS data reveals the differences among their electrochemical properties. It can be concluded that our strategy could efficiently enhance conductivity, improve ion diffusion kinetics, and facilitate the redox reactions leading to good electrochemical performance.

4. CONCLUSIONS

In summary, hierarchical nanostructured Ni-CNTs@β-Ni(OH)$_2$ composites were prepared via a facile chemical method. Ultrathin β-Ni(OH)$_2$ nanoplates were vertically grown on Ni-CNTs. The morphology and content of β-Ni(OH)$_2$ can be controlled by modulating the ratio of $NiCl_2 \cdot 6H_2O$ to Ni-CNTs. Ni-CNTs served as both the growth substrate and 3D conductive network. This hierarchical nanostructure provided remarkable synergistic effects: facilitate electron and ion transport, and accelerate the reversible redox reactions. Benefiting from the synergistic effects, as-prepared Ni-CNTs@β-Ni(OH)$_2$ composites exhibited high electrochemical performance. This strategy has potential for large-scale production and can be applied to the preparation of other hierarchical nanostructured metal hydroxide/oxide composites.

■ ASSOCIATED CONTENT

Supporting Information

XRD spectra of three Ni-CNTs@β-Ni(OH)$_2$ samples; SEM images of sample **c** (500 nm); TEM images of sample **b** (400 nm); SEM images of Ni-CNTs; TGA curves of three Ni-CNTs@β-Ni(OH)$_2$ samples. This material is available free of charge via the Internet at http://pubs.acs.org.

■ AUTHOR INFORMATION

Corresponding Author

*Phone: (+86)-21-51630213. Fax: (+86)-21-51630210. E-mail: rcche@fudan.edu.cn.

Notes

The authors declare no competing financial interest.

■ ACKNOWLEDGMENTS

This work was supported by the Ministry of Science and Technology of China (973 Project Nos. 2013CB932901 and 2009CB930803), and the National Natural Foundation of China (Nos. 11274066, 51172047, 51102050, and U1330118). This project was sponsored by Shanghai Pujiang Program and "Shu Guang" project of Shanghai Municipal Education Commission and Shanghai Education Development Foundation (09SG01).

■ REFERENCES

(1) Wang, G.; Zhang, L.; Zhang, J. A review of electrode materials for electrochemical supercapacitors. *Chem. Soc. Rev.* **2012**, *41* (2), 797–828.

(2) Jiang, J.; Liu, J.; Ding, R.; Zhu, J.; Li, Y.; Hu, A.; Li, X.; Huang, X. Large-Scale Uniform α-Co(OH)$_2$ Long Nanowire Arrays Grown on Graphite as Pseudocapacitor Electrodes. *ACS Appl. Mater. Interfaces* **2010**, *3* (1), 99–103.

(3) Hercule, K. M.; Wei, Q.; Khan, A. M.; Zhao, Y.; Tian, X.; Mai, L. Synergistic Effect of Hierarchical Nanostructured MoO_2/Co(OH)$_2$ with Largely Enhanced Pseudocapacitor Cyclability. *Nano Lett.* **2013**, *13* (11), 5685–5691.

(4) Li, H. B.; Yu, M. H.; Lu, X. H.; Liu, P.; Liang, Y.; Xiao, J.; Tong, Y. X.; Yang, G. W. Amorphous Cobalt Hydroxide with Superior Pseudocapacitive Performance. *ACS Appl. Mater. Interfaces* **2014**, *6* (2), 745–749.

(5) Wang, H.; Casalongue, H. S.; Liang, Y.; Dai, H. Ni(OH)$_2$ Nanoplates Grown on Graphene as Advanced Electrochemical Pseudocapacitor Materials. *J. Am. Chem. Soc.* **2010**, *132* (21), 7472–7477.

(6) Jiang, H.; Zhao, T.; Li, C.; Ma, J. Hierarchical self-assembly of ultrathin nickel hydroxide nanoflakes for high-performance supercapacitors. *J. Mater. Chem.* **2011**, *21* (11), 3818–3823.

(7) Ji, J.; Zhang, L. L.; Ji, H.; Li, Y.; Zhao, X.; Bai, X.; Fan, X.; Zhang, F.; Ruoff, R. S. Nanoporous Ni(OH)$_2$ Thin Film on 3D Ultrathin-Graphite Foam for Asymmetric Supercapacitor. *ACS Nano* **2013**, *7* (7), 6237–6243.

(8) Wu, Z.-S.; Ren, W.; Wen, L.; Gao, L.; Zhao, J.; Chen, Z.; Zhou, G.; Li, F.; Cheng, H.-M. Graphene Anchored with Co_3O_4 Nanoparticles as Anode of Lithium Ion Batteries with Enhanced Reversible Capacity and Cyclic Performance. *ACS Nano* **2010**, *4* (6), 3187–3194.

(9) Yuan, C.; Yang, L.; Hou, L.; Li, J.; Sun, Y.; Zhang, X.; Shen, L.; Lu, X.; Xiong, S.; Lou, X. W. Flexible Hybrid Paper Made of Monolayer Co_3O_4 Microsphere Arrays on rGO/CNTs and Their Application in Electrochemical Capacitors. *Adv. Funct. Mater.* **2012**, *22* (12), 2560–2566.

(10) Rakhi, R. B.; Chen, W.; Cha, D.; Alshareef, H. N. Substrate Dependent Self-Organization of Mesoporous Cobalt Oxide Nanowires with Remarkable Pseudocapacitance. *Nano Lett.* **2012**, *12* (5), 2559–2567.

DOI: 10.1021/am5077183
ACS Appl. Mater. Interfaces 2015, 7, 974–979

(11) Meher, S. K.; Justin, P.; Ranga Rao, G. Microwave-Mediated Synthesis for Improved Morphology and Pseudocapacitance Performance of Nickel Oxide. *ACS Appl. Mater. Interfaces* **2011**, *3* (6), 2063−2073.
(12) Xia, X.; Tu, J.; Zhang, Y.; Wang, X.; Gu, C.; Zhao, X.-b.; Fan, H. J. High-Quality Metal Oxide Core/Shell Nanowire Arrays on Conductive Substrates for Electrochemical Energy Storage. *ACS Nano* **2012**, *6* (6), 5531−5538.
(13) Wang, B.; Chen, J. S.; Wang, Z.; Madhavi, S.; Lou, X. W. Green Synthesis of NiO Nanobelts with Exceptional Pseudo-Capacitive Properties. *Adv. Energy Mater.* **2012**, *2* (10), 1188−1192.
(14) Ding, S.; Zhu, T.; Chen, J. S.; Wang, Z.; Yuan, C.; Lou, X. W. Controlled synthesis of hierarchical NiO nanosheet hollow spheres with enhanced supercapacitive performance. *J. Mater. Chem.* **2011**, *21* (18), 6602−6606.
(15) Zhang, G.; Yu, L.; Hoster, H. E.; Lou, X. W. Synthesis of one-dimensional hierarchical NiO hollow nanostructures with enhanced supercapacitive performance. *Nanoscale* **2013**, *5* (3), 877−881.
(16) Wu, Z.-S.; Wang, D.-W.; Ren, W.; Zhao, J.; Zhou, G.; Li, F.; Cheng, H.-M. Anchoring Hydrous RuO_2 on Graphene Sheets for High-Performance Electrochemical Capacitors. *Adv. Funct. Mater.* **2010**, *20* (20), 3595−3602.
(17) Wang, Y.-G.; Wang, Z.-D.; Xia, Y.-Y. An asymmetric supercapacitor using RuO_2/TiO_2 nanotube composite and activated carbon electrodes. *Electrochim. Acta* **2005**, *50* (28), 5641−5646.
(18) Lu, Z.; Chang, Z.; Zhu, W.; Sun, X. Beta-phased $Ni(OH)_2$ nanowall film with reversible capacitance higher than theoretical Faradic capacitance. *Chem. Commun.* **2011**, *47* (34), 9651−9653.
(19) Yang, S.; Wu, X.; Chen, C.; Dong, H.; Hu, W.; Wang, X. Spherical [small alpha]-$Ni(OH)_2$ nanoarchitecture grown on graphene as advanced electrochemical pseudocapacitor materials. *Chem. Commun.* **2012**, *48* (22), 2773−2775.
(20) Ma, X.; Liu, J.; Liang, C.; Gong, X.; Che, R. A facile phase transformation method for the preparation of 3D flower-like [small beta]-$Ni(OH)_2$/GO/CNTs composite with excellent supercapacitor performance. *J. Mater. Chem. A* **2014**, *2* (32), 12692−12696.
(21) Jiang, H.; Li, C.; Sun, T.; Ma, J. High-performance supercapacitor material based on $Ni(OH)_2$ nanowire-MnO_2 nanoflakes core-shell nanostructures. *Chem. Commun.* **2012**, *48* (20), 2606−2608.
(22) Zhou, W.; Cao, X.; Zeng, Z.; Shi, W.; Zhu, Y.; Yan, Q.; Liu, H.; Wang, J.; Zhang, H. One-step synthesis of Ni_3S_2 nanorod@$Ni(OH)_2$ nanosheet core-shell nanostructures on a three-dimensional graphene network for high-performance supercapacitors. *Energy Environ. Sci.* **2013**, *6* (7), 2216−2221.
(23) Fan, Z.; Yan, J.; Wei, T.; Zhi, L.; Ning, G.; Li, T.; Wei, F. Asymmetric Supercapacitors Based on Graphene/MnO_2 and Activated Carbon Nanofiber Electrodes with High Power and Energy Density. *Adv. Funct. Mater.* **2011**, *21* (12), 2366−2375.
(24) Zhang, L. L.; Xiong, Z.; Zhao, X. S. A composite electrode consisting of nickel hydroxide, carbon nanotubes, and reduced graphene oxide with an ultrahigh electrocapacitance. *J. Power Sources* **2013**, *222* (0), 326−332.
(25) Huang, L.-M.; Wen, T.-C.; Gopalan, A. Electrochemical and spectroelectrochemical monitoring of supercapacitance and electrochromic properties of hydrous ruthenium oxide embedded poly(3,4-ethylenedioxythiophene)−poly(styrene sulfonic acid) composite. *Electrochim. Acta* **2006**, *51* (17), 3469−3476.
(26) Sharma, R. K.; Rastogi, A. C.; Desu, S. B. Manganese oxide embedded polypyrrole nanocomposites for electrochemical supercapacitor. *Electrochim. Acta* **2008**, *53* (26), 7690−7695.
(27) Dreyer, D. R.; Park, S.; Bielawski, C. W.; Ruoff, R. S. The chemistry of graphene oxide. *Chem. Soc. Rev.* **2010**, *39* (1), 228−240.
(28) Hu, G.; Li, C.; Gong, H. Capacitance decay of nanoporous nickel hydroxide. *J. Power Sources* **2010**, *195* (19), 6977−6981.
(29) Yuan, A.; Cheng, S.; Zhang, J.; Cao, C. Effects of metallic cobalt addition on the performance of pasted nickel electrodes. *J. Power Sources* **1999**, *77* (2), 178−182.
(30) Snook, G. A.; Duffy, N. W.; Pandolfo, A. G. Evaluation of the effects of oxygen evolution on the capacity and cycle life of nickel hydroxide electrode materials. *J. Power Sources* **2007**, *168* (2), 513−521.
(31) Yan, J.; Fan, Z.; Sun, W.; Ning, G.; Wei, T.; Zhang, Q.; Zhang, R.; Zhi, L.; Wei, F. Advanced Asymmetric Supercapacitors Based on $Ni(OH)_2$/Graphene and Porous Graphene Electrodes with High Energy Density. *Adv. Funct. Mater.* **2012**, *22* (12), 2632−2641.
(32) Song, H.-K.; Hwang, H.-Y.; Lee, K.-H.; Dao, L. H. The effect of pore size distribution on the frequency dispersion of porous electrodes. *Electrochim. Acta* **2000**, *45* (14), 2241−2257.
(33) Liu, H.; He, P.; Li, Z.; Liu, Y.; Li, J. A novel nickel-based mixed rare-earth oxide/activated carbon supercapacitor using room temperature ionic liquid electrolyte. *Electrochim. Acta* **2006**, *51* (10), 1925−1931.
(34) Sun, W.; Zheng, R.; Chen, X. Symmetric redox supercapacitor based on micro-fabrication with three-dimensional polypyrrole electrodes. *J. Power Sources* **2010**, *195* (20), 7120−7125.

DOI: 10.1021/am5077183
ACS Appl. Mater. Interfaces 2015, 7, 974−979